# Accepted Manuscript

An anisotropic inelastic constitutive model to describe stress softening and permanent deformation in arterial tissue

Eoghan Maher, Arthur Creane, Caitríona Lally, Daniel J. Kelly

Please cite this article as: Maher, E., Creane, A., Lally, C., Kelly, D.J., An anisotropic inelastic constitutive model to describe stress softening and permanent deformation in arterial tissue. *Journal of the Mechanical Behavior of Biomedical Materials* (2012), doi:10.1016/j.jmbbm.2012.03.001

This is a PDF file of an unedited manuscript that has been accepted for publication. As a service to our customers we are providing this early version of the manuscript. The manuscript will undergo copyediting, typesetting, and review of the resulting proof before it is published in its final form. Please note that during the production process errors may be discovered which could affect the content, and all legal disclaimers that apply to the journal pertain.

# An anisotropic inelastic constitutive model to describe stress softening and permanent deformation in arterial tissue

Eoghan Maher[1], Arthur Creane[2], Caitríona Lally[1,2], Daniel J. Kelly[1]

1. Trinity Centre for Bioengineering, School of Engineering, Trinity College, Dublin, Ireland.

2. School of Mechanical and Manufacturing Engineering, Dublin City University, Dublin, Ireland.

Corresponding author:

Dr. Daniel Kelly,

Trinity Centre for Bioengineering,

School of Engineering,

Trinity College,

Dublin,

Ireland.

Ph +353-1-8963947   Fax +353-1-6795554

E-mail: kellyd9@tcd.ie

## Abstract

Inelastic phenomena such as softening and unrecoverable inelastic strains induced by loading have been observed experimentally in soft tissues such as arteries. These phenomena need to be accounted for in constitutive models of arterial tissue so that computational models can accurately predict the outcomes of interventional procedures such as balloon angioplasty and stenting that involve non-physiological loading of the tissue. In this study, a novel constitutive model is described that accounts for inelastic effects such as Mullins-type softening and permanent set in a fibre reinforced tissue. The evolution of inelasticity is governed by a set of internal variables. Softening is introduced through a typical continuum damage mechanics approach, while the inelastic residual strains are introduced through an additive split in the stress tensor. Numerical simulations of aorta and carotid arterial tissue subjected to uniaxial testing in the longitudinal, circumferential and axial directions are used to demonstrate the model's ability to reproduce the anisotropic inelastic behaviour of the tissue. Material parameters derived from best-fits to experimental data are provided to describe these inelastic effects for both aortic and carotid tissue.

## 1. Introduction

Optimisation of vascular medical devices using computational tools such as the finite element method requires accurate constitutive models of arterial tissue. Developing such constitutive models is challenging due to the complex structure and composition of vascular tissue. At physiological levels of pressure, arteries exhibit highly nonlinear, anisotropic and viscoelastic responses to loading (Fung, 1981; Holzapfel et al., 2005). Furthermore, during procedures such as balloon angioplasty and stenting, arteries also experience non-physiological magnitudes of pressure and deformations. At these non-physiological loads arteries display inelastic behaviour as a result of damage to the tissue, which can be observed as a softening of the stress-strain response between loading cycles (Alastrué et al., 2008; Pena et al., 2010). Such structural changes due to tissue damage need be considered when modelling surgical interventions. The damage mechanisms responsible for softening of arterial tissue are not fully understood, however it has been observed that in ligaments damage may occur as a result of tearing or plastic deformation of the fibrous component of the tissue or by a biomechanical degradation of extracellular matrix due to protease release associated with cell necrosis (Provenzano et al., 2002). The softening effect that occurs in fibrous soft tissue has been seen to largely depend on the previous maximum strain that the tissue has experienced. This behaviour is also observed in rubbers and is known as the Mullins effect (Mullins, 1948). Another phenomenon that occurs as a result of non-physiological loading is the presence of residual inelastic strains (or permanent set) on unloading. Both stress softening and permanent set have been observed for other soft tissues: such as skin, brain, venous and vaginal tissue (Ehret and Itskov, 2009; Franceschini et al., 2006; Peña, 2011); as well as arterial tissue (Calvo et al., 2007; Pena et al., 2010) and atherosclerotic plaque (Maher *et al.,* 2011).

The mechanical behaviour of arterial tissue and plaque is commonly described using hyperelastic material models (Delfino et al., 1997; Holzapfel et al., 2000; Lally et al.,

2004; Maher et al., 2009); however these models typically do not incorporate damage effects and as a result are limited when modelling the effects of non-physiological loading during surgical interventions. The Mullins effect theory does not implicitly account for inelastic strains and many damage models omit permanent set from the formulation (Alastrué et al., 2007; Balzani et al., 2006; Calvo et al., 2007; Hokanson and Yazdani, 1997). A number of models have been proposed to describe stress softening in biological tissues. These models are often based on continuum damage mechanics theory; where a reduction factor (Simo and Ju, 1987a; Simo and Ju, 1987b) related to the evolution of irreversible internal variables is applied to model damage to either isotropic (Hokanson and Yazdani, 1997; Maher et al., 2011) or anisotropic models (Alastrué et al., 2007; Balzani et al., 2006; Calvo et al., 2007; Pena and Doblare, 2009). In anisotropic models of soft tissue, damage can either be isolated to the anisotropic fibrous component (Balzani et al., 2006) or applied to both the isotropic matrix and fibrous components separately (Calvo et al., 2007). Hokanson and Yazdani (1997) proposed a model where a 4$^{th}$ order damage tensor was used to induce anisotropic softening to an isotropic material. Other approaches to modelling stress softening include pseudoelastic constitutive models (Franceschini et al., 2006; Pena and Doblare, 2009) or multi-mechanism models that describe failure or deactivation of tissue components (Li and Robertson, 2009; Wulandana and Robertson, 2005). Models of soft tissues have also considered fracture and viscoelastic dissipation in front of the crack tip to describe failure in the tissue (Forsell and Gasser, 2011).

Relatively few constitutive models have been proposed to describe permanent set (Ehret and Itskov, 2009; Franceschini et al., 2006; Gasser, 2011; Gasser and Holzapfel, 2002; Maher et al., 2011; Peña, 2011; Tanaka and Yamada, 1990). Gasser and Holzapfel (2002) proposed a constitutive model for arterial tissue based on multisurface slip plasticity, where plastic deformations are due to slip in the collagen fibre component of the matrix. Tanaka and Yamada (1990) also proposed a plasticity model to account for

permanent set and softening, formulating their model in a viscoplastic framework. Ehret and Itskov (2009) presented a model to describe the dissipative behaviour of soft tissue including softening, permanent set and preconditioning; although this model uses non-standard invariants which results in a complex formulation. Gasser (2011) proposed a multi-scale microfiber approach, modelling collagen fibers as bundles of fibrils with crosslinks between in an isotropic matrix. This model described an approach that coupled a viscoplastic sliding mechanism with failure of the collagen cross-links to model permanent deformation and softening of a collagen fiber. The constitutive behaviour of the fibers is integrated over a unit sphere to determine the macroscopic tissue properties. Peña (2011) used a formulation based on the evolution of internal variables to introduce inelastic softening to the anisotropic components of the model. Franceschini *et al* (2006) adapted a pseudoelastic formulation for particle filled rubbers (Dorfmann and Ogden, 2004; Ogden and Roxburgh, 1999) to model softening and permanent set for brain tissue. Other models have also used a pseudo-elastic based approach to describe inelastic strains in carotid plaque (Maher et al., 2011).

Despite the significant progress that has been made in modelling the mechanical behaviour of arterial tissue, to the authors knowledge to date few models have been proposed to describe anisotropic stress softening and permanent set in arterial tissue (Gasser, 2011; Tanaka and Yamada, 1990). Without considering such phenomena it will not be possible to develop models to accurately predict lumen gain during clinical procedures such as angioplasty and stenting (Early and Kelly, 2011; Early and Kelly, 2010; Early et al., 2009; Pericevic et al., 2009). In this study an anisotropic inelastic constitutive model is formulated to describe stress softening and permanent set for arterial tissue. While stress-softening is commonly applied to the isotropic matrix and anisotropic fiber components (Alastrué et al., 2007; Calvo et al., 2007), models that also incorporate anisotropic permanent set generally only consider it in the fiber component of constitutive

models (Gasser, 2011; Gasser and Holzapfel, 2002; Peña, 2011). Recently we have observed that higher magnitudes of permanent deformations occur in aortic or carotid tissue due to longitudinal tensile strains compared to circumferential tensile strains, with even greater magnitude permanent deformations observed due to radial compressive strains (Maher et al., *in press*), suggesting that the non-collagenous matrix in the artery is more easily damaged than the more circumferentially orientated collagen fibers during loading. In an attempt to describe this complex material behaviour, the objective of this study is to develop a constitutive model of arterial tissue that incorporates stress-softening and permanent deformations in both the isotropic ground matrix and anisotropic fiber components. The formulation is split into an elastic softening, equivalent to the Mullins effect, based on a typical damage mechanics approach and an inelastic softening effect, which results in residual strains, which is based on an additive split of the stress tensor and the irreversible evolution of internal variables. The efficacy of the model is demonstrated by fitting to experimental data.

## 2. Materials and methods

### 2.1. Anisotropic hyperelastic constitutive model

As arterial tissue is generally viewed as a nearly incompressible tissue, a multiplicative decomposition of the deformation gradient tensor, $\mathbf{F} = J^{1/3}\bar{\mathbf{F}}$, and the right Cauchy-Green strain tensor, $\mathbf{C} = J^{2/3}\bar{\mathbf{C}}$, into volumetric (dilatational) and isochoric (volume preserving) parts is performed (Flory, 1961); where $J$ is the determinant of the deformation gradient tensor. This allows a decoupled representation of the strain energy density function $\psi$ to be used.

$$\psi = \psi_{vol}(J) + \psi_{isch}(\bar{\mathbf{C}}, \mathbf{M_0}, \mathbf{N_0}) \qquad \text{(Eqn. 1)}$$

The volumetric term, $\psi_{vol}$ is a function of the determinant of the deformation gradient tensor $J$ and is defined here by the equation, $\psi_{vol} = (\kappa/2)\ln^2 J$ (Holzapfel, 2000). The isochoric part of the strain energy is a function of the modified right Cauchy-Green tensor $\bar{\mathbf{C}}$ and the structural tensors, $\mathbf{M_0} = \mathbf{m_0} \otimes \mathbf{m_0}$ and $\mathbf{N_0} = \mathbf{n_0} \otimes \mathbf{n_0}$ (Spencer, 1971). The structural tensors are functions of the unit vectors in the preferred fibre directions in the undeformed tissue $\mathsf{m}_0$ and $\mathsf{n}_0$, with the square of the stretch in the fibre directions given by the modified invariants $\bar{I}_4$ and $\bar{I}_6$, see Eqn. 2. Other invariants can also be associated with the structural tensors, but are commonly excluded from constitutive formulations due to the difficulty in quantifying them, and are not considered here.

$$\bar{I}_4 = \bar{\mathbf{C}}:\mathbf{M_0} \qquad\qquad \bar{I}_6 = \bar{\mathbf{C}}:\mathbf{N_0} \qquad\qquad \text{(Eqn. 2)}$$

We can now define the 2$^{\text{nd}}$ Piola-Kirchhoff stress $\mathsf{S}$ as:

$$\mathbf{S} = 2\frac{\partial\psi(\mathbf{C},\mathbf{M},\mathbf{N})}{\partial\mathbf{C}} = 2\frac{\partial\psi_{vol}(J)}{\partial J}\frac{\partial J}{\partial\mathbf{C}} + 2\frac{\partial\psi_{isch}(\bar{\mathbf{C}},\mathbf{M},\mathbf{N})}{\partial\bar{\mathbf{C}}}\frac{\partial\bar{\mathbf{C}}}{\partial\mathbf{C}}$$

$$= \mathbf{S}_{vol} + \mathbf{S}_{isch} \qquad\qquad \text{(Eqn. 3)}$$

where $\mathbf{S}_{vol}$ and $\mathbf{S}_{isch}$ are the volumetric and isochoric parts of the stress respectively. The isochoric part of the strain energy density can be split into isotropic and anisotropic components. In structural models this represents anisotropically orientated fibres in an isotropic matrix. Here the isotropic component is described using an exponential function of the modified strain invariant $\bar{I}_1 = tr\bar{\mathbf{C}}$, which has previously been used to model arterial

tissues as isotropic (Delfino et al., 1997; Maher et al., 2011). The anisotropic components are exponential functions of the invariants $\bar{I}_4$ and $\bar{I}_6$ (Holzapfel et al., 2002):

$$\psi_{isch} = \psi_m + \psi_{4,6} = \frac{a}{b}\left(exp\left[\frac{b}{2}(\bar{I}_1 - 3)\right] - 1\right) + \sum_{j=4,6}\frac{k_1}{k_2}\left(exp\left[k_2(\bar{I}_j - 1)^2\right] - 1\right)$$

(Eqn. 4)

$$\mathbf{S}_{isch} = 2\sum_{i=m,4,6}\frac{\partial\psi_i(\bar{I}_i)}{\partial\bar{I}_i}\frac{\partial\bar{I}_i}{\partial\mathbf{C}} = \sum_{i=m,4,6}\bar{\mathbf{S}}_i$$

(Eqn. 5)

where $a$, $b$, $k_1$ and $k_2$ are material parameters evaluated through fitting the model to data from mechanical testing and $\bar{I}_m = \bar{I}_1$. The elasticity tensor in the material description $\mathbb{C}$ is similarly defined:

$$\mathbb{C}_{isch} = 4\sum_{i=m,4,6}\frac{\partial^2\psi_i(\bar{I}_i)}{\partial\mathbf{C}^2} = \sum_{i=m,4,6}\bar{\mathbb{C}}_i$$

(Eqn. 6)

## 2.2. Stress-softening damage model

As is common in continuum damage mechanics theory when applied to soft tissues, damage is assumed to affect only the isochoric part of the constitutive model (Alastrué et al., 2007; Calvo et al., 2007; Simo, 1987). The isochoric stress-softened damaged strain energy density function $\psi_{SS}$ is defined for such materials as:

$$\psi_{SS} = (1 - D_m)\psi_m(\bar{I}_1) + \Sigma_{j=4,6}(1 - D_j)\psi_j(\bar{I}_j) \qquad \text{(Eqn. 7)}$$

where $\psi_m$ is the undamaged strain energy of the isotropic matrix and is a function of the modified first strain invariant. $\psi_j$, $j = 4, 6$ are the strain energy densities of the undamaged anisotropic family of fibres and $(1 - D_i)$, $i = $ m, 4, 6 are scalar functions, known as the reduction factors, that act as internal variables with $D_i \in [0,1]$ defined as damage variables for the matrix ($D_m$) and the two fibre directions ($D_4$ and $D_6$ respectively).

Evaluating the Clausius-Duhem inequality for isothermal conditions, where the internal dissipation $D_{int} = -\dot{\psi} + {}^1/_2 \mathbf{S} : \dot{\mathbf{C}} \geq 0$ and using standard arguments of continuum mechanics (Holzapfel, 2000) the following relationships can be established:

$$\mathbf{S}_{SS} = \sum_{i=m,4,6} 2(1 - D_i)\frac{\partial \overline{\psi_i(\bar{I}_i)}}{\partial \mathbf{C}} = \sum_{i=m,4,6}(1 - D_i)\,\bar{\mathbf{S}}_i \qquad \text{(Eqn. 8)}$$

$$-\frac{\partial \psi}{\partial D_i}\dot{D}_i = \psi_i \dot{D}_i \geq 0 \quad where \quad \psi_i \geq 0 \ \ and \ i = m, 4, 6 \qquad \text{(Eqn. 9)}$$

where $\mathbf{S}_{SS}$ and $\bar{\mathbf{S}}_i$, $i = $ m, 4, 6 are the total isochoric, the isotropic part and the anisotropic parts of the second Piola-Kirchhoff stress respectively. Eqn. 9 shows that the evolution of the damage variables $D_i$ is an irreversible process, where $\psi_i$ are the thermodynamic forces which govern damage evolution.

We now define the strain space based criteria needed for damage evolution at any time during the loading process as (Simo, 1987):

$$\phi_i(\bar{\mathbf{C}}, \Xi_i^m) = \sqrt{2\psi_i(\bar{\mathbf{C}}(t))} - \Xi_i^m \leq 0 \qquad \text{(Eqn. 10)}$$

where $\Xi_i^m(t) = \max_{s=(0,t)} \sqrt{2\psi_i(\bar{\mathbf{C}}(s))}$ and $\Xi_i^t = \sqrt{2\psi_i(\bar{\mathbf{C}}(t))}$ (Eqn. 11)

with the damage criteria $\phi_i$, $i = m, 4, 6$, and the equivalent strain definition $\Xi_i^t$. $\phi_i = 0$ which characterises the damage surface whose normal is defined as $\mathbf{N}_i = \partial\phi_i/\partial\mathbf{C}$. The second criterion is based on the double contraction $\mathbf{N}_i : \dot{\mathbf{C}}$, where $\mathbf{N}_i : \dot{\mathbf{C}} > 0$ describes loading when $\phi = 0$. Evolution of the damage variables $D_i$ can be expressed by

$$\dot{D}_i = \begin{cases} D_i'(\Xi_i)\dot{\Xi}_1, & \text{if } \phi_i = 0 \text{ and } \mathbf{N}_i : \dot{\mathbf{C}} > 0 \\ \\ 0 & \text{otherwise} \end{cases} \quad \text{(Eqn. 12)}$$

where the functions $D_i'(\Xi_i) = \partial D_i/\partial \Xi_i$ characterise damage evolution in the tissue. Making use of the chain rule the isochoric part of the elasticity tensor in the material description $\mathbb{C}_{SS}$ can be derived from the second Piola-Kirchhoff stress tensor in Eqn. 8.

$$\mathbb{C}_{SS} = \mathbb{C}_m + \mathbb{C}_4 + \mathbb{C}_6 \quad \text{(Eqn. 13)}$$

where $\mathbb{C}_i = \begin{cases} (1 - D_i)\bar{\mathbb{C}}_i - \left[\frac{\partial D_i}{\partial \Xi_i}\right]\bar{\mathbf{S}}_i \otimes \bar{\mathbf{S}}_i, & \phi_i = 0 \text{ and } \mathbf{N}_i : \dot{\mathbf{C}} > 0 \\ \\ (1 - D_i)\bar{\mathbb{C}}_i, & \text{otherwise} \end{cases}$ (Eqn. 14)

with $\mathbb{C}_i$ as defined in equation 6. The reduction factors $D_i$ are defined for all equations here as (Miehe, 1995):

$$D_i = d_\infty^i [1 - \exp(-\Xi_i^m/r_i)] \qquad \text{(Eqn. 15)}$$

with $d_\infty^i$ and $r_i$ as material parameters determined through fitting to test data

.

## 2.3. Damage Model with Permanent Deformations

The permanent deformation damage formulation proposed here is characterised by an additive split of the isochoric part of the stress tensor into a stress-softened damaged stress tensor and an inelastic stress tensor $\mathbf{S}_{IN}$ that results in permanent deformations on unloading. The stress-softened damage term, $\mathbf{S}_{SS}$ is defined as in the previous section.

$$\mathbf{S}_{isch} = \mathbf{S}_{SS} - \mathbf{S}_{IN} \qquad \text{(Eqn. 16)}$$

The general form of the isochoric strain energy density function can be written as:

$$\psi_{isch} = \psi_{SS} - \frac{1}{2} \sum_{i=m,4,6} \mathbf{S}_{IN}^i : \bar{\mathbf{C}} \qquad \text{(Eqn. 17)}$$

where $\psi_{SS}$ is as defined in Eqn. 7. The volumetric part of the strain energy is defined as in section 2.1, i.e. $\psi_{vol} = (\kappa/2) \ln^2 J$.

To obtain the stress relation it is necessary to determine the time derivative of the strain energy and evaluate the Clausius-Duhem inequality as in the previous section. This results in the inequality

$$D_{int} = \left( \mathbf{S} - J\frac{\partial \psi_{vol}(J)}{\partial J}\mathbf{C}^{-1} - \sum_{i=m,4,6} J^{-2/3}\mathbb{P}:(1-D_i)2\frac{\partial \psi_i}{\partial \bar{\mathbf{C}}} + \sum_{i=m,4,6} J^{-2/3}\mathbb{P}:\mathbf{S}_{IN}^i \right)$$
$$: \frac{\dot{\mathbf{C}}}{2} + \sum_{i=m,4,6} \psi_i \dot{D}_i + \frac{1}{2}\sum_{i=m,4,6} \bar{\mathbf{C}}:\dot{\mathbf{S}}_{IN}^i \ \geq 0 \qquad \text{(Eqn. 6.18)}$$

from which one can derive the second Piola-Kirchhoff stress tensor $\mathsf{S}$ and the non-negative internal dissipation inequalities. $\mathbb{P} = \mathbb{I} - 1/3\,\mathbf{C}^{-1} \otimes \mathbf{C}$ is the deviatoric projection tensor in the material configuration, where $\mathbb{I}$ is the 4$^{\text{th}}$ order unit tensor. The dissipation inequalities for damage induced permanent deformation are defined in Eqn. 9.

$$\mathbf{S} = \mathbf{S}_{vol} + \sum_{i=m,4,6}(1-D_i)\bar{\mathbf{S}}_i - \sum_{i=m,4,6}\mathbf{S}_{IN}^i \qquad \text{(Eqn. 19)}$$

$$\frac{1}{2}\bar{\mathbf{C}}:\dot{\mathbf{S}}_{IN}^i \geq 0 \qquad \text{(Eqn. 20)}$$

Eqn. 20 shows that $\mathbf{S}_{IN}^i$ act as dissipative tensors such that if the strain applied to the tissue is tensile, i.e. $\bar{C}_{ij} > 0$ than the rate of change of the inelastic stress will be either positive or zero $\dot{S}_{IN_{ij}}^i \geq 0$. The inelastic stresses $\mathbf{S}_{IN}^i$ are therefore dependent on the strain in the tissue and we propose criteria for evolution of the inelastic stresses based on the modified strain invariants:

$$\varphi_i(\bar{\mathbf{C}}, t) = \bar{I}_i(\bar{\mathbf{C}}) - I_i^* \leq 0 \qquad \text{(Eqn. 21)}$$

$$I_i^*(t) = \max_{s=(0,t)} \bar{I}_i(s) \qquad \text{(Eqn. 22)}$$

where $\bar{I}_i$, $i = 1, 4, 6$, are the modified strain invariants of the right Cauchy-Green strain tensor at any given strain and $I_i^*(t)$ are the maximum values of the strain invariants in the history of the material. As the strain energy density is a function of the strain invariants, when $\varphi_i = 0$ from Eqn. 21 we will get $\phi_i = 0$ from the stress-softening damage criterion from Eqn. 10. The normal to the permanent deformation damage surface, described by $\varphi_i = 0$, is defined as $\mathbf{N}_{IN}^i = \partial\varphi_i/\partial\mathbf{C}$. We define the evolution of the internal variables $I_i^*$ and the inelastic stresses as follows:

$$I_i^* = \begin{cases} 2\dfrac{\partial I_i^*}{\partial \mathbf{C}} : \dfrac{\dot{\mathbf{C}}}{2}, & if \ \varphi_i = 0 \ and \ \mathbf{N}_{IN}^i : \dot{\mathbf{C}} \geq 0 \\[2em] 0, & otherwise \end{cases} \qquad \text{(Eqn. 23)}$$

$$\mathbf{S}_{IN}^i = \begin{cases} 2\dfrac{\partial \psi_{IN}^i(I_i^*)}{\partial \mathbf{C}}, & if \ \varphi_i = 0 \ and \ \mathbf{N}_{IN}^i : \dot{\mathbf{C}} \geq 0 \\[2em] constant, & otherwise \end{cases} \qquad \text{(Eqn. 24)}$$

where $\psi_{IN}^i$ are the inelastic dissipated internal strain energies during the loading process for the matrix and family of fibres respectively. The above equations make use of the fact that when the yield criterion for permanent deformation is met $\bar{I}_i = I_i^*$, and thus $\partial I_i^*/\partial\mathbf{C} = \partial\bar{I}_i/\partial\mathbf{C}$, in order to calculate the inelastic stresses. The inelastic dissipated internal strain energy $\psi_{IN}^i$ has the same form as the elastic strain energy density functions,

$$\psi_{IN}^m = \frac{a^*}{b^*}\left(exp\left[\frac{b^*}{2}(I_1^* - 3)\right] - 1\right) \quad \text{(Eqn. 25)}$$

$$\psi_{IN}^j = \frac{k_1^*}{k_2^*}\left(exp\left[k_2^*(I_j^* - 1)^2\right] - 1\right) \quad j = 4, 6 \quad \text{(Eqn. 26)}$$

with $a^*, b^*, k_1^*$ and $k_2^*$ material constants to describe the damage induced permanent deformation effects fitted to mechanical test data. The material elasticity tensor can be defined using the chain rule as:

$$\mathbb{C} = \mathbb{C}_{SS} - \mathbb{C}_{INm} - \mathbb{C}_{IN4} - \mathbb{C}_{IN6} \quad \text{(Eqn. 27)}$$

$$\mathbb{C}_{INi} = \begin{cases} 4\dfrac{\partial^2 \psi_{IN}^i}{\partial \mathbf{C}^2} = 4\dfrac{\partial^2 \psi_{IN}^i}{\partial I_i^* \partial I_i^*}\dfrac{\partial^2 I_i^*}{\partial \mathbf{C}\partial \mathbf{C}}, & \phi_i = 0 \text{ and } \mathbf{N}_i : \dot{\mathbf{C}} > 0 \\[2em] 0 \qquad\qquad, & otherwise \end{cases} \quad \text{(Eqn. 28)}$$

which again makes use of the fact that $\partial I_i^*/\partial \mathbf{C} = \partial \bar{I}_i/\partial \mathbf{C}$ when the yield conditions for permanent deformation are met.

## 2.4. Characterisation of inelastic mechanical response of arteries

The model as presented here is compared to the experimental stress-strain behaviour of porcine aorta and carotid arterial tissue in response to cyclic uniaxial loading experiments conducted by the authors. A strip of tissue in each of the circumferential and longitudinal directions was tested in tension for each artery and cylindrical radial samples were also tested in compression. The tensile strips were approximately 2 mm wide and 10 mm long

for the carotid samples and 3 mm wide and 17 mm long for aortic samples. Displacement-rate controlled cyclic loading was applied to each specimen, with a strain-rate of approximately 0.005 s$^{-1}$. The maximum strain level increasing periodically by 10% every 5 loading cycles to a maximum of 60 %. Testing of the 3.5 mm diameter cylindrical radial compressive samples followed a similar loading regime as the tensile specimens. The experimental methodology is described in full elsewhere (Maher et al., *in press*). Inelastic strains were determined where the stress-strain curve crossed the strain axis on reloading.

The strain energy function defined in equation 17 with associated material constants was fit to the mechanical data of representative samples from samples in the longitudinal and circumferential tensile directions. The fitting procedure used minimised the root mean square (rms) error for the stress-strain response and the inelastic strains as described in a previous study (Maher et al., 2011). The fitting to experimental data was performed numerically: the model presented in section 2.3 was implemented as a user material in the finite element code ABAQUS (Dassault Systèmes, SIMULIA, RI, USA). Tensile boundary conditions were applied to a model to reproduce the experimental tensile loading, as is common in the literature (Balzani et al., 2006; Peña et al., 2011), see Fig. 1. The resulting stress-strain curves in both the circumferential and longitudinal were compared to the experimental data. The fibre orientations were defined by the angle, $\beta$, between the fibres and the circumferential direction. In cylindrical polar coordinates the unit vectors $m_0$ and $n_0$ are defined as (Holzapfel et al., 2000):

$$[\mathbf{m_0}] = \begin{bmatrix} 0 \\ cos\beta \\ sin\beta \end{bmatrix} \qquad [\mathbf{n_0}] = \begin{bmatrix} 0 \\ cos\beta \\ -sin\beta \end{bmatrix} \qquad \text{(Eqn. 29)}$$

where $\beta$ was included as a variable parameter in the model fitting procedure. The fitting procedure was repeated a number of times to ensure a reasonably consistent set of

parameters were produced. The success of the model fits were analysed and model was also used to predict inelastic strains caused by radial compressive loading as a further test to determine how accurately the inelastic damage mechanisms were described by the model.

## 3. Results

The best fit material parameters for the aorta and carotid experimental data are presented in Table 1. The comparison between model predictions and experimental results is illustrated in Figs. 2-5. Good agreement between the experimental data and the model were found when comparing the stress-strain response on loading and reloading, see Fig. 2. The quality of fit was worst in the transition region between low and high stiffness regions, however the fit in these regions was still of reasonably good quality, see Fig. 2. The total *rms* error for the $2^{nd}$ loading cycles in both directions, $\chi_s$ is presented in Table 1 as a measure of the quality of the fit.

To aid clarity of the fit, comparisons for the elastic loading response, or load envelope, are shown in Fig. 3. There is a good quality of fit with the elastic loading in both longitudinal and circumferential directions for both the aorta and carotid artery, see Fig. 3. In addition, good quality fits for the $2^{nd}$ loading curves at each strain level were also achieved for both arteries in both directions, see Fig. 4.

The model was able to accurately predict the softening behaviour in both the longitudinal and circumferential directions, see Fig. 4. The worst quality fits were found at low strains in the circumferential direction for both arteries with the model predicting less softening than observed experimentally. (Only the $2^{nd}$ loading curve is shown to aid clarity in the figure.) The model accurately predicted the magnitude of inelastic strain in the circumferential and longitudinal directions for a range of applied peak strains, see Fig. 5. The only noticeable exception was that inelastic strains in the circumferential direction

were generally overestimated at small strains. This is due to damage initiation occurring when the tissue stretch is beginning in the model. It is likely, as is seen in ligaments, that damage initiation will not occur immediately, particularly in the collagen fibres (Provenzano et al., 2002). Good agreement in the magnitude of inelastic strains observed in the radial direction is found up to approximately 40% compressive strain after which the model tends to over-estimate the inelastic deformations (Fig. 5 e,f). Overall, a good agreement with the experimental data is observed.

## 4. Discussion

In this study, a constitutive model was presented to describe damage and inelastic deformations in vascular tissue. The model was presented in terms of stress-softening damage, which follows the typical continuum damage mechanics structure of modelling the Mullins effect, and damage induced permanent deformations, which is characterised by an additive split of the stress tensor and the evolution of internal variables based on the maximum value of the modified strain invariants in the load history. The use of the additive split in the stress tensor was motivated by a pseudo-elastic constitutive model developed for particle-filled rubbers (Dorfmann and Ogden, 2004) that has been adapted successfully for use in soft tissues (Franceschini et al., 2006). In the pseudo-elastic approach a 2nd term in the strain energy density, which was partially dependent on the maximum stretch, results in an 'additive' negative stress contribution and thus permanent deformations on unloading. We formulated a damage-based model to describe permanent deformations using an additive split in the stress tensor where the occurrence of permanent deformations are defined through the evolution of internal variables based on damage criteria. An additive split in the stress tensor had also been used in modelling plastic flow (Simo and Ju, 1987a).

The model was shown to successfully describe the typical soft tissue damage phenomena of stress softening, with good quality fits for the experimental data obtained. The assumption of independent damage mechanisms existing for the fibres and base matrix also allows the model to predict the anisotropic softening observed in arterial tissue, with the model capturing the smaller inelastic strains observed in the circumferential direction and the larger inelastic strains observed in the longitudinal direction. The values obtained for the inelastic constants, $d_\infty^i$ and $r_i$, suggest that stress-softening occurs in both the matrix and fibres which results in the softening pneumonia observed in both the longitudinal and circumferential directions. The inelastic constants corresponding to the fibres are however smaller than the corresponding constants for the matrix. This results in the lower magnitudes of inelastic strains in the circumferential direction where the stiff, possibly less inelastic fibres have more of an influence. This may indicate that collagen fibres in arterial tissue act to constrain the inelastic deformations that are hypothesised to occur more prominently in the other constituents, e.g. elastin, smooth muscle or ground matrix. It should be noted however that as a phenomenological model the fibre directions here do not represent true collagen fibre families and are merely a representation of the overall anisotropic behaviour of the arteries which limits the insight into individual arterial component behaviour the model may provide.

The exact mechanisms through which damage occurs in arterial tissue is unknown, but for example failure of crosslinks between fibres might result in a softening effect while failure or slip of the fibres in the matrix might result in permanent deformations. Such damage mechanisms have been hypothesised by Parry et al (1978) where non-recoverable creep is prevented through non-covalent crosslinks between fibres and matrix and small diameter fibres result in more of these links as they provide a greater surface area per unit mass. They further hypothesise that large diameter fibres maximise covalent intrafibrillar crosslinks thereby increasing the stiffness of the tissue (Parry *et al.*, 1978). The model

presented here could possibly be modified to include the effects of cross-linking on the damage behaviour using a multi-scale approach (Tang et al., 2009). Tang et al (2009) presented a multi-scale model of the collagen fiber components of a tissue. The deformation gradient of the collagen fiber is multiplicatively decomposed into an elasto-plastic uniaxial fiber deformation and the remaining purely elastic shear deformation. The flow resistance in the fibrils is modified by a parameter based on the cross-linking density and thus cross-linking effects the plastic flow of the fibrils. The strain-energy function based on the mechanics of the fibrils and matrix of the fiber is presented in terms of the first and fourth strain invariants of the elastic strain for the fibrils and of the total uniaxial fiber strain for the matrix. A similar strain-energy density could be formulated for the uniaxial fiber deformation with the invariants based on the total uniaxial fiber deformation. When applying a damage model such as presented here, a parameter for cross-linking density as used by Tang *et al.* (2009) could be used to modify the damage surface in the model which would have an effect on the rate at which damage occurs. The breaking of non-covalent crosslinks resulting in slip of collagen fibres in the matrix has been used to describe inelastic deformations in arterial tissue (Gasser and Holzapfel, 2002). The mechanisms of damage in the matrix are made more complex due to the number of components that it consists of. The elastin network contains intrafibrillar crosslinks that also contribute to the stiffness in the artery (Greenwald, 2007). Damage of these links may induce softening, while slip or damage of other components may result in permanent set. The constitutive model developed as part of this study describes the damage effects as energy dissipation which occurs discontinuously during loading as damage progresses.

There are few models in the literature that account for both softening and permanent set. The ability to account for both these behaviours gives the proposed model an advantage over models that describe the Mullins effect based on traditional continuum damage mechanics. Considering permanent deformation is particularly important in the

case of vascular tissue where the end goal of many surgical interventions is to increase the final lumen size through mechanical loading. Models that have been fit to experimental data for other soft tissues that include softening and permanent set (Ehret and Itskov, 2009; Franceschini et al., 2006; Peña, 2011) also have the potential to be used for arterial tissue. In these models permanent set has been applied to either uniaxial deformation alone (Franceschini et al., 2006), to only the fiber component of the model (Gasser, 2011; Gasser and Holzapfel, 2002; Peña, 2011) or both in and orthogonal to the fiber direction (Ehret and Itskov, 2009). From the experimental data it is observed that the permanent deformations in the less stiff longitudinal direction are greater than those due to loading in the circumferential direction (Maher et al., *in press*), with even greater magnitudes of permanent deformation observed due to radial compressive strains. Such material behaviour may be difficult to replicate using models that apply damage induced permanent deformations to the fibers only. While constitutive models have been used successfully to capture the stress-softening behaviour of arterial tissue using a fiber-damage only approach (Balzani et al., 2006), the further introduction of permanent deformation only applied to the fibers would likely result in greater magnitude permanent deformation in the circumferential direction due to the fibers orientating towards the stiffer circumferential direction. Whether other models recently described in the literature can be used to describe this complex material behaviour while maintaining physiologically consistent fiber angles is worthy of further investigation (Ehret and Itskov, 2009; Gasser, 2011; Peña, 2011).

There are several limitations to the constitutive model presented in this study. The model fit to the experimental data is not as accurate in describing the high strain behaviour (last cycle) as for lower strain levels. This is possibly a result of the greater contribution of the adventitia at higher strain levels experimentally and the difficulty in capturing this behaviour when modelling the artery wall as a single layer. The damage processes are described using a phenomenological model and as such it is difficult to relate the inelastic

constants to a physical meaning. Viscoelasticity is not considered and would likely play a role in the softening effect. In the experimental data the unloading and subsequent reloading curves are not coincident (i.e. a hysteresis effect) as in the idealised Mullins effect, which is likely due to viscoelastic behaviour. In the context of this model, where the Mullins effect is modelled as an irreversible damage induced stress-softening based on continuum damage mechanics, we feel it is more appropriate to fit to the 2nd loading curve than the unloading curve due to the observation that the softening effect between unloading and reloading appears to be an irreversible effect caused by damage while the further softening between the reloading and unloading curves appears to be a reversible viscoelastic process. As the model is fit to the reloading curve the unloading behaviour is not accurately characterized in cases where significant differences between unloading and reloading occur. Failure is also not considered here. Failure behaviour was omitted as tissue failure was generally absent from the experimental model used in this study. Failure could be included into the stress-softening damage variables $D_i$ by introducing a maximum value of the equivalent strain measure $\Xi_i^m$ above which $D_i = 1$ (Calvo et al., 2007; Pena et al., 2009). Preconditioning effects could be added to the model through the introduction of a continuous damage mechanism (Pena et al., 2009).

Preliminary testing was undertaken to confirm that the residual strains observed in porcine arterial tissue on unloading remain after an unloaded rest period of between 1 and 2 hours. It is possible however that significant viscoelastic recovery occurs over a longer period of time or that viscous behaviour may be more significant in other tissues and/or species. For example viscoelasticity has been observed to be important in fracture models of ventricular tissue (Forsell and Gasser, 2011). It would be possible to introduce a viscous effect to modify the permanent deformations by modifying the inelastic stress tensor $S_{IN}$ to incorporate non-equilibrium stresses, similar to viscoelastic models in the literature (Pena et al., 2010; Peña et al., 2008; Simo, 1987). One example of this sort of formulation would

be a strain energy density function defined as $\psi_{isch} = \psi_{SS} - 1/2\sum_{i=m,4,6}((\mathbf{S}_{IN}^i - \mathbf{Q}_i):\bar{\mathbf{C}} + \psi_l(\mathbf{Q}_i))$, where the non-equlibrium stress $\mathbf{Q}_i$ is related to (Eqn. 24) in this study rather than the term $2\,(\partial\psi_0/\partial\bar{\mathbf{C}})$ as in typical viscoelastic theory (Peña et al., 2008). In this formulation we would have a peak original inelastic effect characterized by $\mathbf{S}_{IN}^i$ which is reduced over time by the non-equilibrium stress. This type of formulation is made easier to implement due to the additive split already implemented in the stress tensor.

Using the tensile data the model can predict inelastic strains due to radial compression with good accuracy at low to medium strains. At high strains however the inelastic strains are overestimated. It has been seen that arteries behave as nearly incompressible materials during arterial expansion (Carew et al., 1968). However the compressive stresses will be comparatively small during the expansion of a healthy artery and it may be possible that at higher magnitudes of radial compression the assumption of near-incompressibility is no longer valid. This may explain the increase in damage and overestimation of compressive stresses that occurs at high strains. However as circumferential tension is the dominant loading mechanism during arterial expansion during procedures such as angioplasty and stenting these high compressive strains may not be reached.

Despite these limitations the model could predict the experimental behaviour of healthy arterial tissue with good accuracy. The constitutive model is one of the few inelastic models that have been fit to arterial tissue experimental data that considers both softening and inelastic strains. The modelling of these inelastic effects allows for more accurate finite element analyses of interventions such as balloon angioplasty or stenting by accounting for tissue damage during loading and hence the resulting lumen gain.

## Acknowledgements

# References

Alastrué, V., E. Peña, *et al.*, 2008. Experimental study and constitutive modelling of the passive mechanical properties of the ovine infrarenal vena cava tissue. Journal of Biomechanics 41, 3038-3045.

Alastrué, V., J.F. Rodríguez, *et al.*, 2007. Structural damage models for fibrous biological soft tissues. International Journal of Solids and Structures 44, 5894-5911.

Balzani, D., J. Schröder, *et al.*, 2006. Simulation of discontinuous damage incorporating residual stresses in circumferentially overstretched atherosclerotic arteries. Acta Biomaterialia 2, 609-618.

Calvo, B., E. Pena, *et al.*, 2007. An uncoupled directional damage model for fibred biological soft tissues. Formulation and computational aspects. Int. J. Numer. Meth. Engng. 69, 2037-2057.

Carew, T.E., R.N. Vaishnav, *et al.*, 1968. Compressibility of the arterial wall. Circ Res 23, 61-68.

Delfino, A., N. Stergiopulos, *et al.*, 1997. Residual strain effects on the stress field in a thick wall finite element model of the human carotid bifurcation. Journal of Biomechanics 30, 777-786.

Dorfmann, A., R.W. Ogden, 2004. A constitutive model for the Mullins effect with permanent set in particle-reinforced rubber. International Journal of Solids and Structures 41, 1855-1878.

Early, M., D. Kelly, 2011. The consequences of the mechanical environment of peripheral arteries for nitinol stenting. Medical and Biological Engineering and Computing, 1-10.

Early, M., D.J. Kelly, 2010. The role of vessel geometry and material properties on the mechanics of stenting in the coronary and peripheral arteries. Proceedings of the Institution of Mechanical Engineers. Part H 224, 465-476.

Early, M., C. Lally, *et al.*, 2009. Stresses in peripheral arteries following stent placement: a finite element analysis Computer Methods in Biomechanics and Biomedical Engineering 12, 25-33.

Ehret, A.E., M. Itskov, 2009. Modeling of anisotropic softening phenomena: Application to soft biological tissues. International Journal of Plasticity 25, 901-919.

Flory, P.J., 1961. Thermodynamic relations for high elastic materials. Transactions of the Faraday Society 57, 829-838.

Forsell, C., T.C. Gasser, 2011. Numerical simulation of the failure of ventricular tissue due to deep penetration: the impact of constitutive properties. J Biomech 44, 45-51.

Franceschini, G., D. Bigoni, *et al.*, 2006. Brain tissue deforms similarly to filled elastomers and follows consolidation theory. Journal of the Mechanics and Physics of Solids 54, 2592-2620.

Fung, Y.C., 1981. Biomechanics : mechanical properties of living tissues / Y.C. Fung. Springer-Verlag, New York :.

Gasser, T.C., 2011. An irreversible constitutive model for fibrous soft biological tissue: A 3-D microfiber approach with demonstrative application to abdominal aortic aneurysms. Acta Biomater.

Gasser, T.C., G.A. Holzapfel, 2002. A rate-independent elastoplastic model for biological fiber-reinforced composites at finite strains:continuum basis,algorithmic formulation and finite element implementation. Computational Mechanics 29, 340-360.

Greenwald, S.E., 2007. Ageing of the conduit arteries. The Journal of Pathology 211, 157-172.

Hokanson, J., S. Yazdani, 1997. A constitutive model of the artery with damage Mechanics Research Communications 24, 151-159.

Holzapfel, G.A., 2000. Nonlinear Solid Mechanics. John Wiley & Sons.

Holzapfel, G.A., C.T. Gasser, *et al.*, 2000. A New Constitutive Framework for Arterial Wall Mechanics and a Comparative Study of Material Models. Journal of Elasticity 61, 1-48.

Holzapfel, G.A., G. Sommer, *et al.*, 2005. Determination of layer-specific mechanical properties of human coronary arteries with nonatherosclerotic intimal thickening and related constitutive modeling. Am J Physiol Heart Circ Physiol 289, H2048-2058.

Holzapfel, G.A., M. Stadler, *et al.*, 2002. A Layer-Specific Three-Dimensional Model for the Simulation of Balloon Angioplasty using Magnetic Resonance Imaging and Mechanical Testing. Annals of Biomedical Engineering 30, 753-767.

Lally, C., A.J. Reid, *et al.*, 2004. Elastic behavior of porcine coronary artery tissue under uniaxial and equibiaxial tension. Ann Biomed Eng 32, 1355-1364.

Li, D., A.M. Robertson, 2009. A structural multi-mechanism damage model for cerebral arterial tissue. J Biomech Eng 131, 101013.

Maher, E., A. Creane, *et al.*, 2009. Tensile and compressive properties of fresh human carotid atherosclerotic plaques. J Biomech 42, 2760-2767.

Maher, E., A. Creane, *et al.*, 2011. Inelasticity of Human Carotid Atherosclerotic Plaque. Ann Biomed Eng.

Maher, E., M. Early, *et al.*, *in press*. Site Specific Inelasticity of Arterial Tissue. J Biomech.

Miehe, C., 1995. Discontinuous and continuous damage evolution in Ogden-type large-strain elastic materials. European Journal of Mechanics, A/Solids 14, 697-720.

Mullins, L., 1948. Effect of Stretching on the Properties of Rubber, Vol 21. RUBDIV, 281-300 pp.

Ogden, R.W., D.G. Roxburgh, 1999. A pseudo-elastic model for the Mullins effect in filled rubber. Proc Roy Soc London A 455.

Parry, D.A.D., G.R.G. Barnes, *et al.*, 1978. A Comparison of the Size Distribution of Collagen Fibrils in Connective Tissues as a Function of Age and a Possible Relation between Fibril Size Distribution and Mechanical Properties. Proceedings of the Royal Society of London. Series B. Biological Sciences 203, 305-321.

Peña, E., 2011. Prediction of the softening and damage effects with permanent set in fibrous biological materials. Journal of the Mechanics and Physics of Solids 59, 1808-1822.

Pena, E., V. Alastrue, *et al.*, 2010. A constitutive formulation of vascular tissue mechanics including viscoelasticity and softening behaviour. J Biomech 43, 984-989.

Peña, E., B. Calvo, *et al.*, 2008. On finite-strain damage of viscoelastic-fibred materials. Applications to soft biological tissues. International Journal for Numerical Methods in Engineering 74, 1198-1218.

Pena, E., M. Doblare, 2009. An anisotropic pseudo-elastic approach for modelling Mullins effect in fibrous biological materials. Mech Res Com 36, 784-790.

Peña, E., P. Martins, *et al.*, 2011. Mechanical characterization of the softening behavior of human vaginal tissue. Journal of the mechanical behavior of biomedical materials 4, 275-283.

Pena, E., J.A. Pena, *et al.*, 2009. On the Mullins effect and hysteresis of fibered biological materials: A comparison between continuous and discontinuous damage models. International Journal of Solids and Structures 46, 1727-1735.

Pericevic, I., C. Lally, *et al.*, 2009. The influence of plaque composition on underlying arterial wall stress during stent expansion: The case for lesion-specific stents. Medical Engineering & Physics 31, 428-433.

Provenzano, P.P., D. Heisey, *et al.*, 2002. Subfailure damage in ligament: a structural and cellular evaluation. J Appl Physiol 92, 362-371.

Simo, J.C., 1987. On a fully three-dimensional finite-strain viscoelastic damage model: Formulation and computational aspects. Computer Methods in Applied Mechanics and Engineering 60, 153-173.

Simo, J.C., J.W. Ju, 1987a. Strain- and stress-based continuum damage models--I. Formulation. International Journal of Solids and Structures 23, 821-840.

Simo, J.C., J.W. Ju, 1987b. Strain- and stress-based continuum damage models - II. Computational aspects. Int J Solids Structures 7, 841-869.

Spencer, A.J.M., 1971. Theory of Invariants, In: Eringen, A.C. (Ed.) Continuum Physics. Academic Press, pp. 240-253.

Tanaka, E., H. Yamada, 1990. An inelastic constitutive model of blood vessels. Acta Mech 82, 21-30.

Tang, H., M.J. Buehler, *et al.*, 2009. A constitutive model of soft tissue: from nanoscale collagen to tissue continuum. Ann Biomed Eng 37, 1117-1130.

Wulandana, R., A.M. Robertson, 2005. An inelastic multi-mechanism constitutive equation for cerebral arterial tissue. Biomech Model Mechanobiol 4, 235-248.

Figure Legends

Fig. 1: Schematic of the finite element model geometry and boundary conditions for circumferential (left) and longitudinal (right) tensile tests. Arrows represent direction of loading and $\beta$ the angle between the collagen fibre and the circumferential direction.

Fig. 2: Comparison between constitutive model fit and experimental results for the stress-strain response in the longitudinal ((a) and (b)) and circumferential ((c) and (d)) for aorta and carotid tissue samples respectively.

Fig. 3: Comparison of stress-strain response predicted by the model with experimental data of the load envelope for (a) aorta and (b) carotid arteries in the circumferential and longitudinal directions.

Fig. 4: Experimental and model comparison of stress-strain curve for the 2$^{nd}$ loading cycle at each strain level in longitudinal (a) aorta and (b) carotid samples; and circumferential (c) aorta and (d) carotid samples. Insets show close-up of the experimental data only so that the permanent deformation can be clearly observed; the red data point in the insets corresponds to the zero stress-state of each loading cycle.

Fig. 5: Inelastic strain on unloading from various peak strains in the longitudinal (a, b), circumferential (c, d) and radial (e, f) directions for aorta (a, c, e) and carotid artery (b, d, f) respectively.

Table 1: Optimised material parameters for aortic and carotid specimens

Aorta

| $a(MPa)$ | $b$ | $k_1(MPa)$ | $k_2$ | $d_\infty^m$ | $r_m$ | $d_\infty^f$ |
|---|---|---|---|---|---|---|
| 0.035 | 3.5 | 0.0125 | 0.7 | 0.7 | 0.16 | 0.9 |
| $r_f$ | $a^*(MPa)$ | $b^*$ | $k_1^*(MPa)$ | $k_2^*$ | $\beta$(degrees) | $\chi_s$ |
| 0.15 | 0.0034 | 0.001 | 0.0001 | 0.0001 | 20 | 0.082 |

Carotid

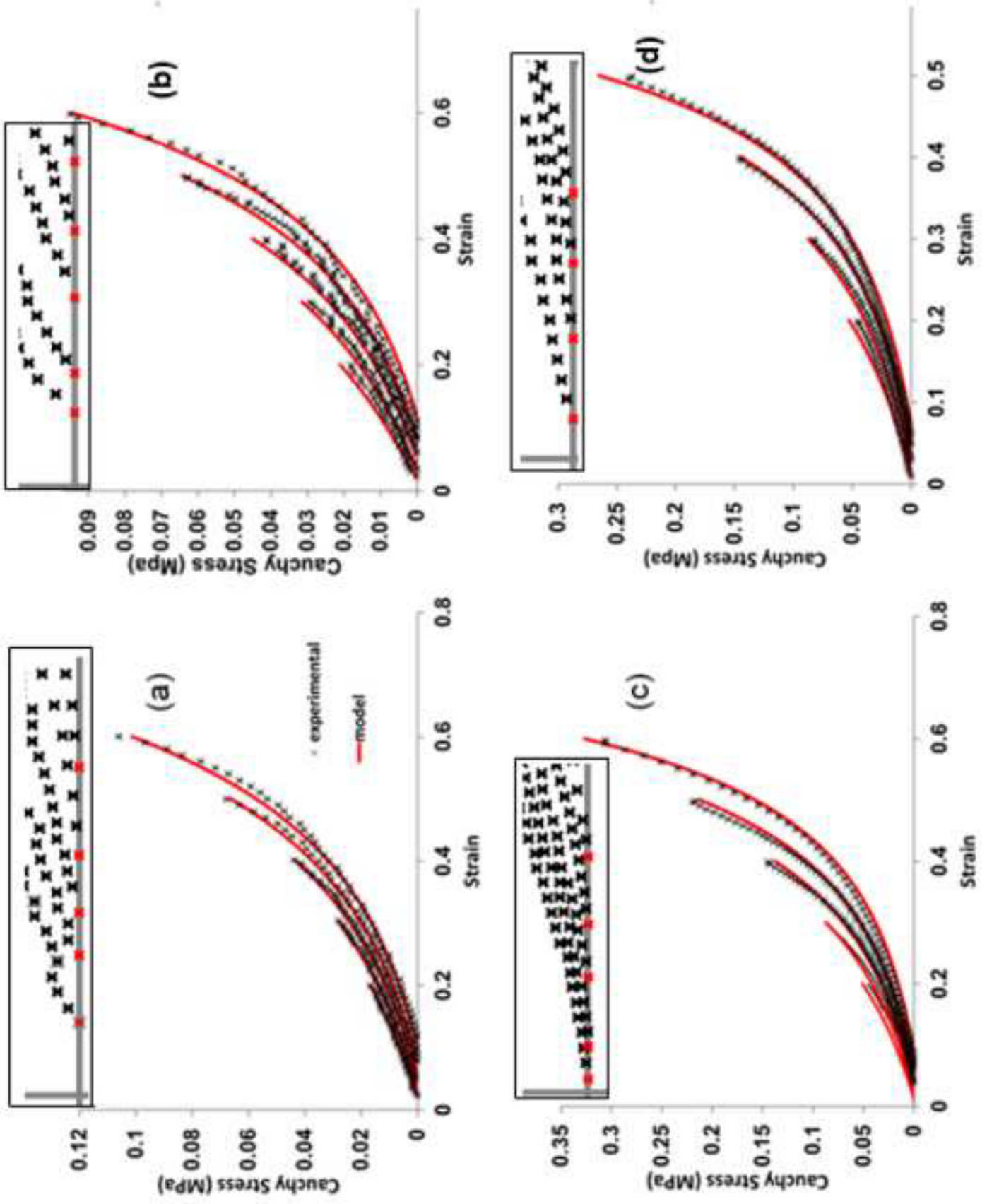| $a(MPa)$ | $b$ | $k_1(MPa)$ | $k_2$ | $d_\infty^m$ | $r_m$ | $d_\infty^f$ |
|---|---|---|---|---|---|---|
| 0.05 | 3.2 | 0.011 | 0.95 | 0.8 | 0.13 | 0.75 |
| $r_f$ | $a^*(MPa)$ | $b^*$ | $k_1^*(MPa)$ | $k_2^*$ | $\beta$(degrees) | $\chi_s$ |
| 0.08 | 0.0035 | 0.001 | 0.0002 | 0.0001 | 15 | 0.037 |
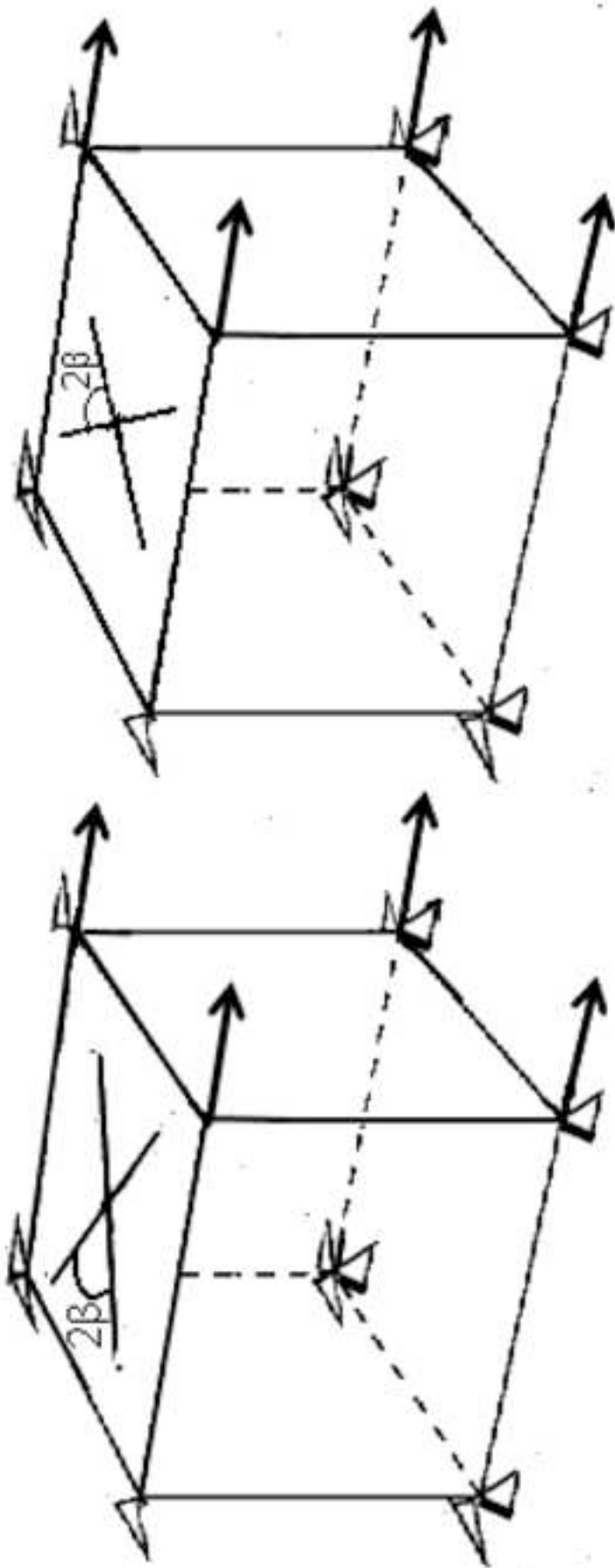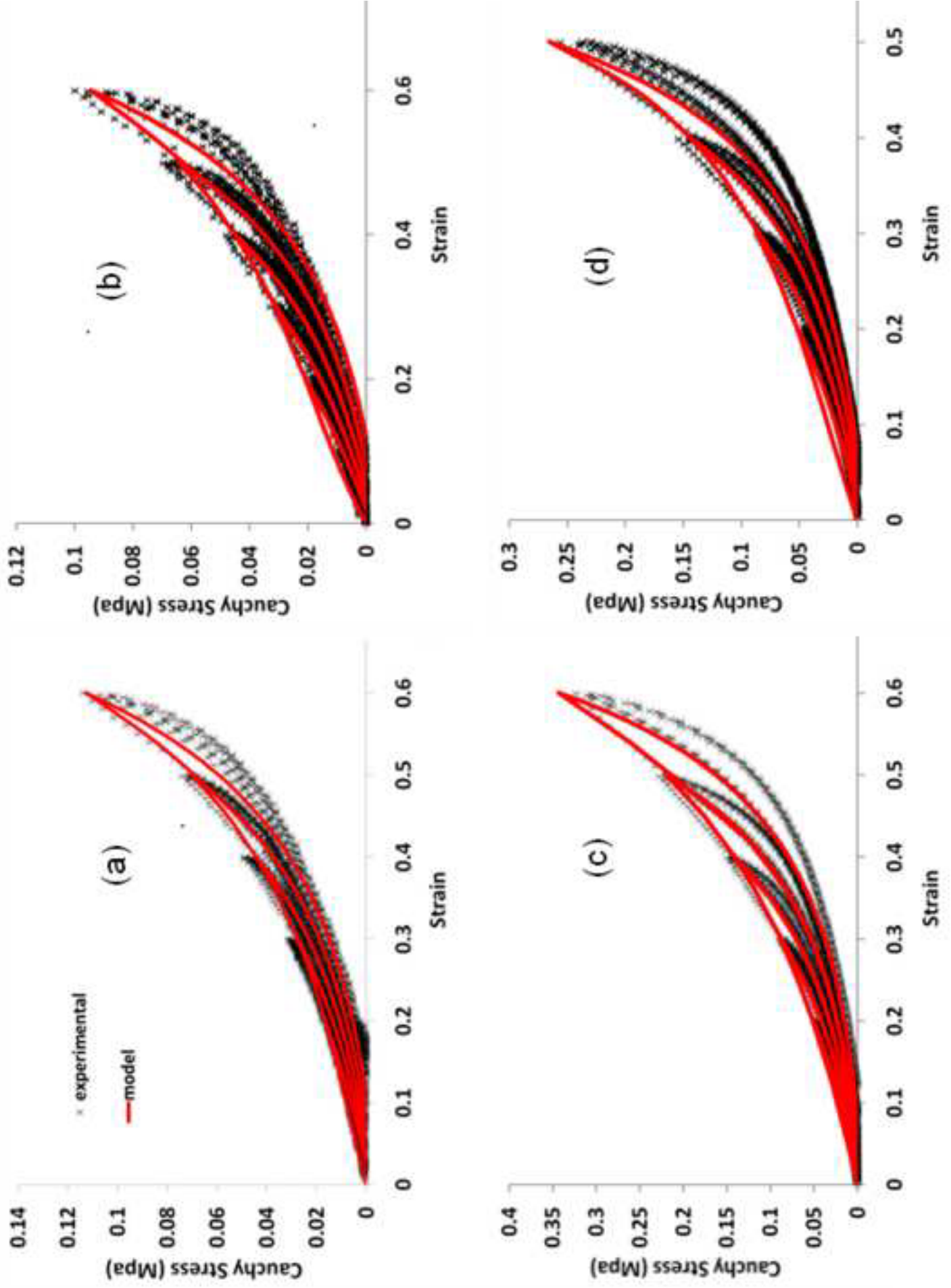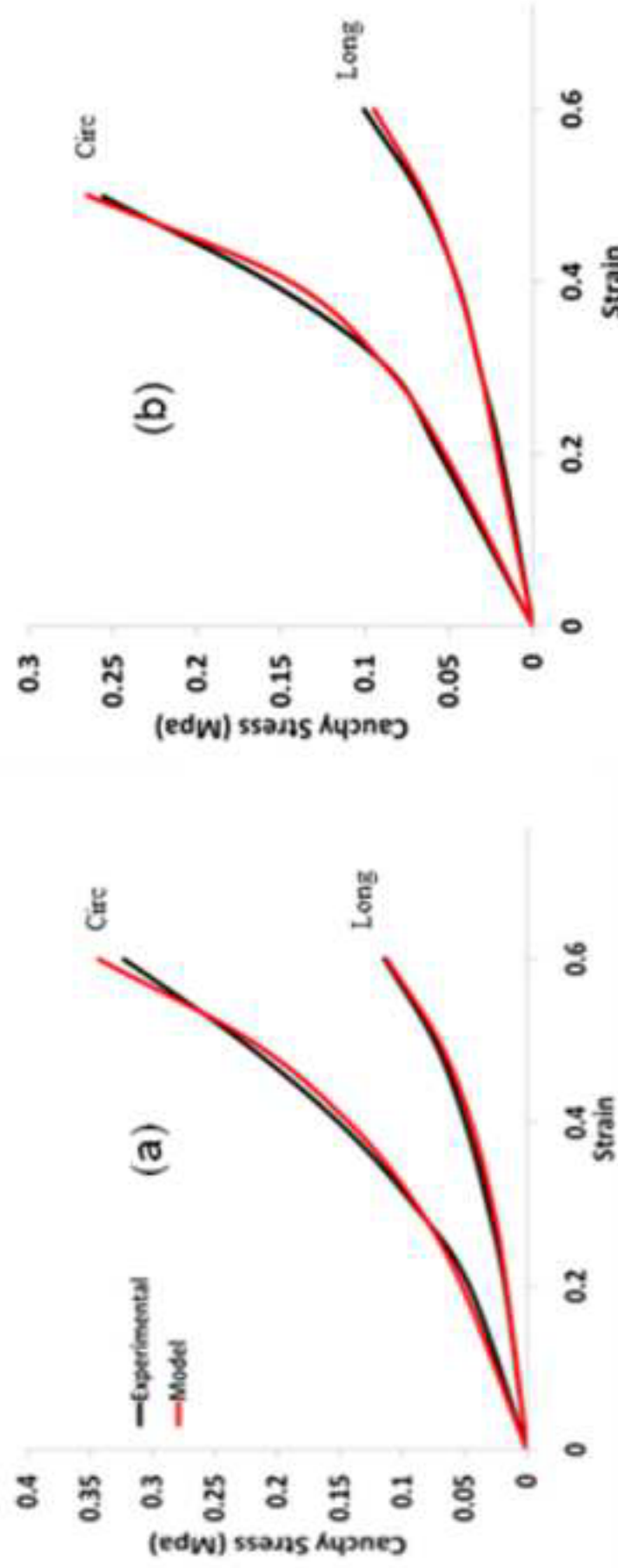
**Figure 5**
Click here to download high resolution image